ADVANCED MATERIALS TECHNOLOGIES
www.advmattechnol.de

Polymer Dielectrics for 3D-Printed RF Devices in the K_a Band

*Michael Lis, Maxwell Plaut, Andrew Zai, David Cipolle, John Russo, Jennifer Lewis, and Theodore Fedynyshyn**

The combination of crowded spectrum and the requirement for high-bandwidth communications has created a need for communications in the K_a radio frequency (RF) band (26.5–40 GHz). Satellite communications, in particular, are increasingly moving over to this band as lower frequency bands become more crowded. These higher frequency bands also have the advantage of allowing for smaller antenna device and waveguide sizes, which are an advantage for low size, weight and power (SWaP) systems. High resolution 3D printing would be an attractive tool for the fabrication of this class of device, except for a lack of appropriate materials to use in this field. With these low-SWaP devices, however, comes the need for high precision fabrication methods. Casting and injection molding can create precision parts, but at significant up-front cost and a limited materials selection, with little flexibility for changes in design. Machining can produce high quality, customized designs, but machining the polymeric and ceramic materials used for high-frequency devices can be difficult and laborious. Additive manufacturing techniques are well placed to fill this space with the ability to fabricate high-resolution devices with high reproducibility. 3D printing can also produce shapes and structures not easily achievable by those other methods. For 3D printing to become widely used for millimeter (30+ GHz) devices, low lost 3D-printabe materials must be developed. Several recent papers have highlighted the versatility of 3D-printed radio devices, but nearly all of these reports cover frequency ranges in the X band (8–12 GHz) or below.[1–4] One paper has addressed terahertz range devices using reflectarrays, in part to avoid transmission loss.[5] Most polymers used in additive manufacturing have significant dipole moments, which contribute to dielectric loss in this regime.[6] This paper presents the creation of low-loss dielectric materials for 3D printing high-frequency radio devices.

Styrenic block copolymers (SBCs), triblock copolymers containing polystyrene end blocks and an aliphatic midblock, are widely used in melt adhesives, automotive parts, and many other commercial applications. The most common varieties of this polymer are polystyrene-block-polybutadiene-block-polystyrene (SBS), polystyrene-block-polyethylene-ran-polybutaline-block-polystyrene (SEBS), and polystyrene-block-polyisoprene-block-polystyrene (SIS). In all three cases, the polymer blocks phase separate upon annealing, leaving a styrenic phase with a glass transition temperature (T_g) well above ambient and an aliphatic phase with a T_g well below ambient.[7] With the polystyrene blocks entangling and holding the polymers together, this system then becomes a thermoplastic elastomer. SBCs have been used as dielectric actuators[8,9] or as a base for polymer-ceramic nanocomposites,[10–12] but measurements of the dielectric properties of these materials have generally been in the sub-gigahertz regime.

This communication describes the creation of printable inks made from styrenic block copolymers and demonstrates the ability to print these inks with nozzles ranging from 10–200 µm. To reduce the shrinkage of samples due to solvent evaporation, the aromatic solvents are replaced with monomers, which are then cross-linked using UV light during the printing process. The dielectric properties of printed objects are measured across the K_a band, establishes their viability as low-loss dielectric materials. As a demonstration of the utility of these printable inks, simple waveguide resonator filters and a lens are created, and their responses measured.

Direct writing of polymeric materials requires an ink capable of being extruded through a nozzle while maintaining shape once deposited. Previous studies have demonstrated this through rapid solvent evaporation,[13] ceramic colloidal gels,[14–18] fiber formation,[19,20] hydrogel networks[21,22] or rapid photopolymerization.[23,24] The former is limited to high-surface area environments, while the rest require materials and chemistries that exhibit RF loss. Highly concentrated solutions of both polystyrene and SBCs have been shown to be highly shear thinning—a trait that provides low viscosity at high shear rates (e.g., passing through a narrow nozzle) and high viscosity at low shear rates (e.g., when deposited).[25,26]

The SBS and SIS-based inks contain 55 wt% block copolymer dispersed in toluene. The SEBS-based ink contains 45 wt% block copolymer dispersed in xylenes. Dispersing the SEBS ink in toluene produced the classic sharkskin effect in the ink after it exits the nozzle while printing.[27,28] It was found that replacing the toluene with xylenes as a solvent greatly reduced this effect. The cause of this difference is not entirely clear, but it is likely related to the improved solubility of the ethylene/butylene midblock in the more aliphatic xylenes. For comparison, polystyrene inks were similarly prepared, with 70% low-molecular-weight (M_w = 110 kDa) polystyrene and 35% high-molecular-weight (M_w = 2000 kDa), respectively, in toluene.

Dr. M. Lis, M. Plaut, Dr. A. Zai, D. Cipolle, J. Russo, Dr. T. Fedynyshyn
MIT Lincoln Laboratory
Lexington, MA 02420, USA
E-mail: Fedynyshyn@ll.mit.edu
Prof. J. Lewis
Harvard School of Engineering and Applied Science and Wyss Institute for Biologically Inspired Engineering
Cambridge, MA 02138, USA

DOI: 10.1002/admt.201600027

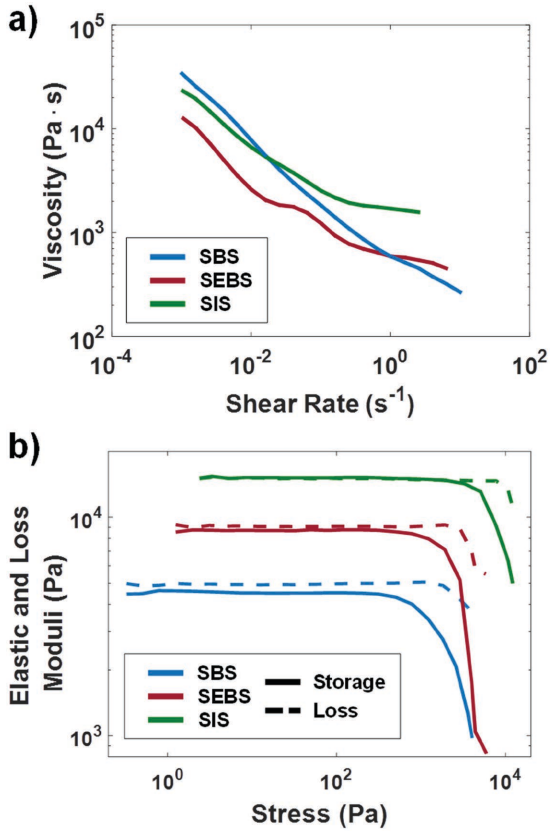

Figure 1. Rheological properties of block copolymer inks containing 55% SBS in toluene, 45% SEBS in xylenes, and 55% SIS in toluene. a) Viscosities of the block copolymer inks under continuous shear flow. All three inks are shear thinning across the measured ranges. b) Shear storage (solid lines) and loss (dashes) moduli of the block copolymer inks under amplitude modulated oscillatory shear. The drop-offs in modulus values mark the yield stress of the materials.

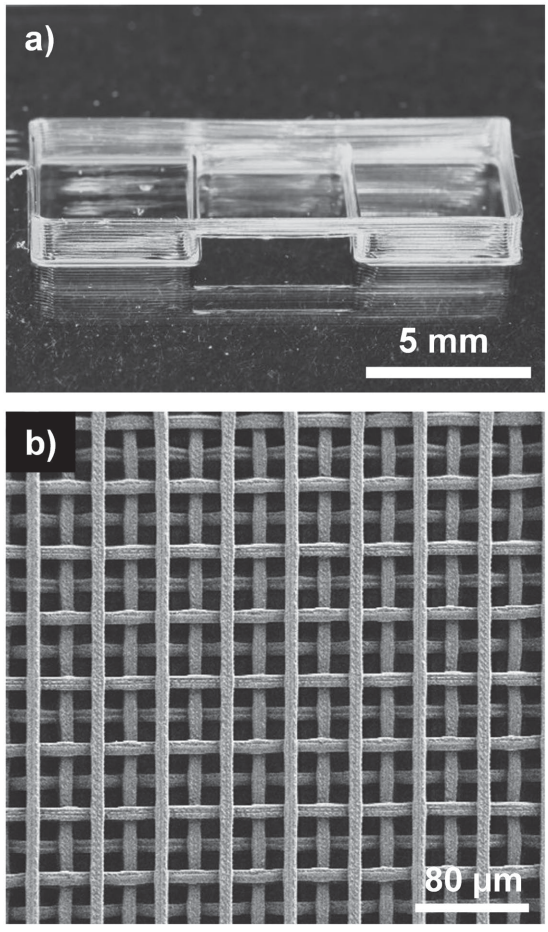

Figure 2. Demonstration structures printed with block copolymer inks. a) Suspended bridge structure with a 5 mm span (SBS ink, 200 µm nozzle). b) FCC woodpile (SEBS ink, 10 µm nozzle). Scale bar is 80 µm.

Figure 1 shows the rheological properties of the three SBC inks. Modulus values and yield stresses are given in Table S2 (Supporting Information). As shown in Figure 1a, both materials are highly shear thinning, showing a near two orders of magnitude drop in viscosity over the measured range. As an example, the SEBS ink has a viscosity of 13 000 Pa·s at very low shear rates, while having a viscosity of only 280 Pa·s, allowing for ready flow of the ink. Both inks show G′/G″ ratios near 1 and yield stresses of 784 Pa for the SBS ink, 2070 Pa for the SIS Ink, and 1072 Pa for the SEBS ink (Figure 1b), giving the inks enough stiffness to support their own weight during printing and allows for layer-by-layer fabrication. Once the ink exits the nozzle, rapid drying improves these elastic properties of the ink further, allowing for the printing of self-supported structures. By comparison, the polystyrene inks, shown in Figure S1 in the Supporting Information, had little shear thinning properties, showing mostly Newtonian behavior until high shear rates.

Immediately after printing, the printed ink is soft and tacky, easily deformed by touch. Despite the apparent softness of the material, it was still possible to print a 5 mm suspended bridge structure (**Figure 2**a) with a 200 µm nozzle. The outer skin of the structure quickly hardened, while full drying of the sample took hours or days, depending on sample thickness. To show resolution possibilities, structures were also printed with a 10 µm nozzle. Figure 2b shows a face-centered cubic (FCC) woodpile, printed with the SEBS ink. The solids content was reduced from 45% to 43% SEBS in xylenes for printing at this resolution, as it allowed for smoother features. Other than this change, no modifications were made to the ink formulation to allow printing at this dimension. The use of the softer ink at these dimensions does not inhibit the printing of suspended structures because features at this dimension have a very high surface area to volume ratio, resulting in rapid drying. As can be seen, though, there is still some submicron scale texturing on the printed lines themselves.

While this approach to printing is well suited to thin-walled structures like that shown in Figure 2a, solvent evaporation leads to anisotropic shrinkage of thicker printed objects (Figure S2, Supporting Information). To ameliorate these effects, the aromatic solvents used in the inks were replaced with a curable monomer mixture. UV curing has been previously combined with direct writing[23,24] but the curable polyurethanes used in that system have too much dielectric loss to use here. The polymerizable mixture used here consists of styrene, divinylbenzene, and the UV photoinitator Irgacure 819 (**Figure 3**a). For the purposes of this paper, these inks are designated X-SBS

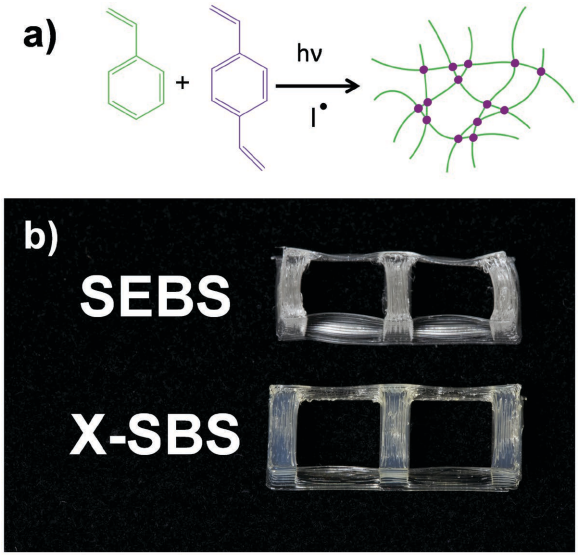

Figure 3. Crosslinkable ink printing. a) Aromatic monomers are replaced with styrene and divinylbenzene monomers, which form cross-linked polystyrene after exposure to UV light. b) Objects printed with the SEBS and X-SBS inks, highlighting the difference in shrinkage.

(crosslinked styrene-butadiene-styrene) and X-SIS (crosslinked styrene-isoprene-styrene). The overall polymer concentrations are similar to before, as are the rheological properties, which are outlined in Table S2 in the Supporting Information. To polymerize the ink immediately following printing, two fiber optic cables, connected to a UV lightbox, were placed around the printhead (Figure S3, Supporting Information).

This printing process resulted in printed samples with noticeably reduced shrinkage (Figure 3b). While the SEBS ink-based sample had noticeable warping on the corners and a trapezoidal effect on the solid blocks, the X-SBS sample has little of either effect. This allows for much more accurate printing of structures than would otherwise be possible without accounting for shrinkage in the object design.

With the printability of these inks established across a range of designs and dimensions, we then sought to determine their dielectric properties. The most critical component of a dielectric material is its electric permittivity, which has both real and imaginary parts that vary with the frequency of the input wave

$$\varepsilon(\omega) = \varepsilon'(\omega) - i\varepsilon''(\omega) \tag{1}$$

Where ε'/e_0 is the dielectric constant, ε'' is the imaginary component, and ω is the frequency of the alternating electric field. The dielectric constant determines how easily the material polarizes in response to an electric field. This also determines the propagation rate of a wave through the material. Furthermore, the ratio of real and imaginary components gives the loss tangent

$$\tan(\delta) = \frac{\varepsilon''}{\varepsilon'} \tag{2}$$

Which allows us to determine the power loss in the material for a propagating wave

Table 1. Results of dielectric testing for various materials.

Polymer	Dielectric constant ε'	Loss tangent $\varepsilon''/\varepsilon' \times 10^3$	Loss relative to Rexolite
Rexolite	2.50	0.52	100%
SEBS	2.52	0.45	86%
SBS	2.43	2.28	441%
SIS	2.28	1.64	317%
X-SBS	2.09	2.26	437%
X-SIS	2.17	1.95	378%

$$P = P_0\, e^{-\tan(\delta)kz} \tag{3}$$

Where P_0 is the initial power, $k = 2\pi/\lambda$ where λ is the wavelength in the propagating medium, and z is the depth of the sample.[29]

In order to be useful dielectric materials, they must have low loss in the desired frequency range. As a standard comparison, a solid piece of Rexolite 1422, a common low-loss dielectric material, was machined to fit a waveguide, and its dielectric constant and loss were measured. SEBS, SBS, and SIS were all 3D printed by solvent casting to the desired waveguide dimensions and were then fit into the waveguide. The dielectric properties of the different polymeric materials are summarized in **Table 1**. The loss values of the block copolymers were measured against the value for Rexolite, as a way of determining the practical viability of these polymers as low-loss dielectrics at 34 GHz. The SBS polymer had a loss value of 2.28×10^{-3}, ≈4.4 times that of Rexolite. The SIS polymer had a slightly lower loss value of 1.64×10^{-3}, 3.2 times the value of Rexolite. The SEBS had the best loss value, 0.45×10^{-3}, even lower than Rexolite. This difference is likely due to the presence of vinyl groups in the midblock of the SBS and SIS polymers, which contribute resonance that leads to loss. The cross-linked inks, again 3D printed by solvent casting to the desired waveguide dimensions, showed very similar loss values and a similar trend, indicating that there was little difference between the cross-linked and uncross-linked materials from a dielectric properties perspective.

As a demonstration of these printable dielectrics, simple waveguide filters were printed. The first, a three-block filter (top of **Figure 4**a), was printed using the uncross-linked SEBS ink. The blocks act as resonators for the radio waves passing through the sample, producing a band-pass filter that allows signal between 30 and 36 GHz to pass through, but blocks other frequencies. Figure 4b (dotted line) shows the expected output of the device by finite element analysis simulation. To avoid some of the complications caused by shrinkage due to solvent loss, a 5 block device was printed, and the end blocks trimmed off. Much of the curling effects seen in Figure 3b were then limited to those removed outer blocks, leaving us with a usable device.

This structure was then placed inside a rectangular waveguide and the signal transmission and reflectance were both measured across the K_a band. As can be seen in Figure 4b, there is good agreement between the expected output of the device and the measured transmission. In both the simulation and the measured data, the center of the high transmission region

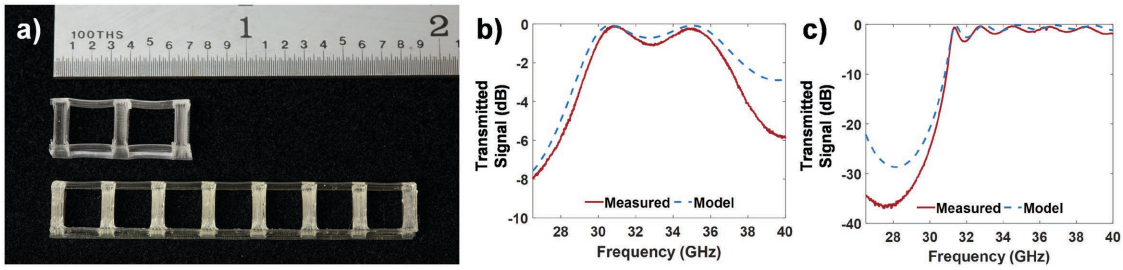

Figure 4. Printed filter devices. a) Three- and eight-block filter devices printed from SEBS and X-SBS inks, respectively. b) Transmission of the three-block filter device. The blue dotted line represents a finite element analysis model based on the filter dimensions. The red solid line is the actual measurement. c) Transmission of the eight-block filter device.

is at 32.8 GHz. While the simulation shows a −3 dB cutoff at 28.8 GHz and never quite achieving a −3 dB cutoff on the other side, the actual device has a narrower pass band, with −3 dB cutoffs at 29.0 and 37.4 GHz. The SEBS ink, therefore, is capable of being printed into a simple waveguide resonator filter device.

The X-SBS ink was then used to print a larger, eight-block high-pass waveguide filter. Transmission was measured identically to the three-block device. Again, we have excellent agreement between the expected output and actual measurement. The device has a 3dB cutoff at about 31.7 GHz, and signal is below −25 dB between 26.5 and 30 GHz. Again, the out of band signal is lower than in the simulation, with a minimum of −36 dB, compared to −29 dB for the simulation. The likeliest explanation for this discrepancy is that the simulation does not fully account for the destructive interference caused by the filter. Since this feature is present in both the 3 stage and 8 stage filters, and that the finished filters outperform the simulations, it was assumed that the fault of the discrepancy lay with the simulation, rather than the finished product.

As a final demonstration, both of the printing versatility of this system as well as its material properties, an antenna meant to fit on the end of a rectangular waveguide was printed (**Figure 5**). The design (Figure 5a, detailed specifications in Figure S4, Supporting Information) consisted of two components. The first is a curved, cylindrical lens 10 mm long and with a radius of curvature of 4.55 mm. The second is a 2 cm barrel that is 600 µm thick on the bottom half and 400 µm thick on the top half. The change in thickness provides a notch to mount the antenna on the end of the waveguide. The design of the antenna produces practical challenges for any printing method. Maintaining the curvature of the lens is paramount, and warping and distortion of the lens would lead to an altered refracted image. Furthermore, the rectangular barrel must remain as thin as possible, so as to not alter the transmission of the radio waves before they reach the lens. To maintain this high-quality surface, a curved printing substrate was printed using an SLA printer. The curved basin matched the curvature of the lens exactly, so that the lens could be printed directly inside the surface (Figure 5b). To facilitate removal of the antenna from the base, a mold release spray was used. Second, the antenna barrel presented an extremely thin, high aspect ratio feature. While the inks are able to support their own weight, any shrinkage at all causes a distortion of the corners, which quickly leads to collapse of the barrel as the printer continues laying material on top of the print defects. To prevent any rounding of the corners, "wings" are added to the sides of the barrel of the lens (Figure 5b). These were trimmed off of the device after printing to yield the final antenna device (Figure 5c).

The radiation pattern of this antenna was modeled in the finite element simulation software HFSS at 30 GHz (Figure 5d, blue line). Figure S5 (Supporting Information) shows the electric field pattern in detail. The lens was mounted on the end of a waveguide (Figure S6, Supporting Information), and the signal output was measured from −90 to 90 degrees in front of the antenna. The measured output from the antenna is represented by the red line (Figure 5d). The black line is the control, the signal coming out of the waveguide without any antenna mounted. The forward signal is boosted by 2.1 dB over the unaltered signal. The antenna also produces significant side lobes, along interference-driven nulls between the lobes and

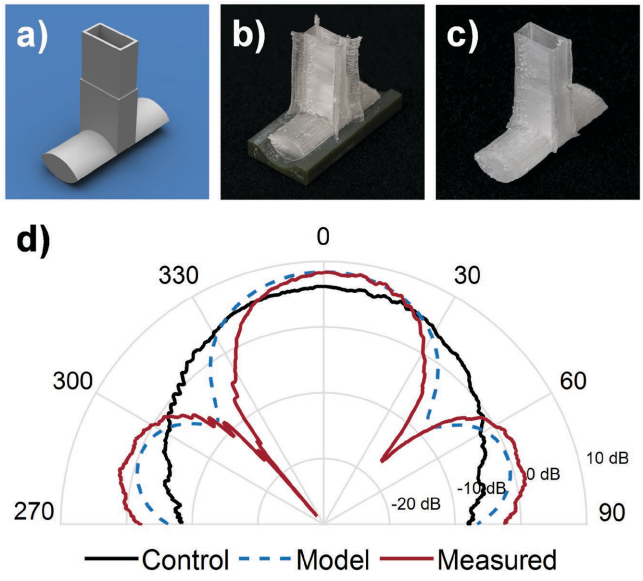

Figure 5. 3D-printed antenna device. a) Rendered design of the antenna. Detailed specifications for the antenna are shown in Figure S5 in the Supporting Information. b) Printed antenna (clear) on top of curved base (green). The "wings" on the side of the barrel exist to prevent curling of the corners. c) Final antenna device, after removal from the base and trimming of the wings. d) Far-field measurement at 30 GHz of the antenna, with signal measured in dBi. The black line represents the control signal from the WR-28 waveguide. The blue line is the modeled output of the antenna design. The red line is the measured output of the antenna.

the center signal. The output of the antenna closely matches the model. There are, however, some minor differences in the angle of the nulls between the measured (±41°) and simulated (±45°) outputs. This is due to small dimensional variations between the printed antenna and the original design. In particular, shrinkage of the SIS ink due to solvent evaporation after printing increases the radius of curvature of the lens slightly, which in turn moves the angle of the nulls slightly inward.

We have demonstrated the ability to 3D print functional RF devices intended for use in the K_a band. Printable inks were created by dissolving styrenic triblock copolymers in aromatic solvents. These SBC inks were found suitable for printing a range of structures, and solidified upon solvent evaporation. To reduce the amount of shrinkage due to solvent loss, crosslinkable inks were created that are polymerized during the printing process. The dielectric constants and the loss tangents of printed blocks were measured, demonstrating that these polymers were low loss, and viable options for K_a band dielectric devices. Two waveguide filter devices were created, and each performed as specified. An antenna was printed, which demonstrated the versatility of this printing process for making devices that would otherwise be difficult to manufacture.

Experimental Section

Materials: SBS (432490), SIS (432415), SEBS (200565), low-molecular-weight polystyrene (110k PS, 430102), styrene, divinylbenzene, toluene, and xylenes were all acquired from Sigma-Aldrich, Milwaukee WI. High-molecular-weight polystyrene (2M PS, PS61111) was purchased from Pressure Chemical Company, Milwaukee WI. All materials were used as purchased without further modification. 3 mL polypropylene luer-lock syringes, 200 and 600 µm polypropylene, luer-lock, tapered syringe tips, and HP3 high pressure adapter were all purchased from Nordson EFD, Westlake OH. Glass 10 µm tips were purchased from World Precision Instruments, Sarasota, FL. Brytac aluminum foil-backed Teflon film was produced by Saint Gobain, Worcester MA.

Molecular Weight Characterization: Polymer molecular weights were determined by gel permeation chromatography in tetrahydrofuran with a Waters 2695 Separations Module with a refractive index detector using polystyrene standards.

Ink Formulation: Printable inks were created by combining polymer with an aromatic solvent in a Speedmixer DAC 400 planetary mixer (Flaktek, Landrum SC). SBS and SIS inks were created by combining 55 wt% polymer with toluene, SEBS ink by combining 45% polymer with xylenes, 110k PS ink by combining 70 wt% polymer with toluene, and the 2M PS ink by combining 35 wt% polymer with toluene. Mixtures were loaded into the mixer and spun at 2350 RPM for three cycles of 10 min.

The crosslinkable inks were formulated similarly to the standard SBC inks described above. Instead of toluene or xylenes, an 88:10:2 wt% mixture of styrene:divinylbenzene:Irgacure 819 was combined in an amber vial. This mixture was added to either 57 wt% SBS or 52 wt% SIS for the X-SBS and X-SIS inks, respectively.

Ink Rheology: Inks were characterized by an AR-2000EX Rheometer (TA Instruments, New Castle, DE) using a 40 mm cone-and-plate geometry. Modulus and yield stress were determined by an amplitude sweep at a frequency of 10 rad s^{-1}. Yield stress was defined as the point where the value of the storage modulus dropped to 90% of the plateau value. Shear thinning rheology was demonstrated by measuring viscosity at a wide range of steady shear rates.

3D Printing: Inks were loaded into 3 mL luer-lock polypropylene syringes. The syringes were capped at the top and bottom and centrifuged at 3100 rpm for 12 min to press the ink to the bottom of the barrel and remove air bubbles. The caps were then removed and the syringe was placed in an HP7x high pressure adapter and mounted to the head of a 3-axis positioning stage (Aerotech Inc., Pittsburgh PA). Material was extruded through tapered, luer-lock polypropylene syringe tips using the HP7X. Air pressure to the HP7x was supplied by an Ultimus V pressure control box (Nordson EFD) connected to the house air supply.

Crosslinkable inks were printed under direct UV exposure. An Omnicure S2000 (Excelitas, Waltham MA) was used as the light source. A dual-headed fiber optic cable was held in place around the print head to allow for immediate exposure of the printed material. To prevent polymerization of the ink inside the syringe tip, the tip was painted black with nail polish and covered in foil.

The antenna base was printed in an Envisiontec Aureus SLA printer. The print included a reference marker on one corner to assist in tip placement. The antenna design was created in SolidWorks and the print path was processed using Slic3r. To easily remove the printed antenna, MR311 mold release spray (Sprayon Products, Cleveland OH) was applied before printing. The antenna was then printed inside the base, using the SIS ink and the methods above.

Dielectric Property Measurement: Complex dielectric permittivity was measured using a rectangular waveguide and a Keysight E8364C Vector Network Analyzer (VNA). Printed or melt-cast slabs of dielectric between one-half and a few wavelengths were placed inside a 2 inch length of split-block waveguide. Measurements were made in the K_a band (26.5 to 40 GHz). The VNA was calibrated using known WR-28 waveguide standards, with inside dimensions of 0.280″ × 0.140″. Dielectric constant and loss values were taken as the median value across the K_a band. Rexolite 1422 (C-Lec Plastics, Philadelphia, PA) was used as a reference for a commercial low-loss material.

Waveguide Filter Device Measurement: Filter devices were measured on identical equipment. Three and eight block resonator filter devices were printed and placed inside a split WR-28 waveguide, and signal transmission through the waveguide was measured from 26.5–40 GHz. Expected filter response was calculated by finite element analysis using HFSS (Version 16.0.0, Ansys, Inc. Pittsburgh, PA) and compared with the actual result.

Antenna Measurement: The antenna was mounted on the end of a WR-28 waveguide (Figure S6, Supporting Information) in a large anechoic chamber (MI Technologies, Suwanee GA). Antenna output at 30 GHz was measured across a range of angles, from –90° to 90°. Expected antenna response was calculated using HFSS.

Supporting Information

Supporting Information is available from the Wiley Online Library or from the author.

Acknowledgements

This work was sponsored by the Assistant Secretary of Defense for Research & Engineering under Air Force Contract number FA8721-05-C-0002. Opinions, interpretations, conclusions, and recommendations are those of the authors, and not necessarily endorsed by the United States Government.

Received: February 18, 2016
Revised: April 8, 2016
Published online:

[1] M. Liang, W. R. Ng, K. Chang, K. Gbele, M. E. Gehm, H. Xin, *IEEE Trans. Antennas Propag.* **2014**, *62*, 1799.

[2] M. Liang, W. R. Ng, K. Chang, M. E. Gehm, H. Xin, *Microw. Symp. Dig. (MTT) 2011 IEEE MTT- Int.* **2011**, 1.

[3] T. P. Ketterl, Y. Vega, N. C. Arnal, J. W. I. Stratton, E. A. Rojas-Nastrucci, M. F. Córdoba-Erazo, M. M. Abdin, C. W. Perkowski, P. I. Deffenbaugh, K. H. Church, T. M. Weller, *IEEE Trans. Microw. Theory Tech.* **2015**, *63*, 4382.
[4] Y. Arbaoui, V. Laur, A. Maalouf, P. Quéffélec, D. Passerieux, A. Delias, P. Blondy, *IEEE Trans. Microw. Theory Tech.* **2016**, *64*, 271.
[5] P. Nayeri, M. Liang, R. A. Sabory-García, M. Tuo, F. Yang, M. Gehm, H. Xin, A. Z. Elsherbeni, *IEEE Trans. Antennas Propag.* **2014**, *62*, 2000.
[6] M. N. Afsar, *IEEE Trans. Instrum. Meas.* **1987**, *IM-36*, 530.
[7] J. G. Drobny, in *Handbook Thermoplastic Elastomers* (Ed: J. G. Drobny), William Andrew Publishing, Norwich, NY, USA **2007**, pp. 161–177.
[8] R. Shankar, T. K. Ghosh, R. J. Spontak, *Adv. Mater.* **2007**, *19*, 2218.
[9] R. Shankar, T. K. Ghosh, R. J. Spontak, *Soft Matter* **2007**, *3*, 1116.
[10] D. J. Carastan, N. R. Demarquette, A. Vermogen, K. Masenelli-Varlot, *Rheol. Acta* **2008**, *47*, 521.
[11] W.-C. Chen, S.-M. Lai, C.-M. Chen, *Polym. Int.* **2008**, *57*, 515.
[12] E. Helal, N. R. Demarquette, L. G. Amurin, E. David, D. J. Carastan, M. Fréchette, *Polymer* **2015**, *64*, 139.
[13] S.-Z. Guo, F. Gosselin, N. Guerin, A.-M. Lanouette, M.-C. Heuzey, D. Therriault, *Small* **2013**, *9*, 4118.
[14] J. E. S. Lewis, J. Stuecker, J. Cesarano, *J. Am. Ceram. Soc.* **2006**, *89*, 3599.
[15] W. W. Michna, J. A. Lewis, *Biomaterials* **2005**, *26*, 5632.
[16] T. J. Ober, D. Foresti, J.A. Lewis, *Proc. Natl. Acad. Sci. USA* **2015**, *112*, 12293.
[17] T. J. O. Hardin, A. D. Valentine, J. A. Lewis, *Adv. Mater.* **2015**, *27*, 3279.
[18] J. C. Smay, J. A. Lewis, *Langmuir* **2002**, *18*, 5429.
[19] S. T. P. Ghosh, X. Wang, D. L. Kaplan, J. A. Lewis, *Adv. Funct. Mater.* **2008**, *18*, 1883.
[20] P. D. Parker, J. Amsden, J. Bressner, J. A. Lewis, D. L. Kaplan, F. G. Omenetto, *Adv. Mater.* **2009**, *21*, 2411.
[21] R. A. Barry III, R. F. Shepherd, J. N. Hanson, R. G. Nuzzo, P. Wiltzius, J. A. Lewis, *Adv. Mater.* **2009**, *21*, 2407.
[22] R. L. T. Kolesky, A. S. Gladman, T. A. Busbee, K. A. Homan, J. A. Lewis, *Adv. Mater.* **2014**, *26*, 3124.
[23] L. L. Lebel, B. Aissa, M. A. E. Khakani, D. Therriault, *Adv. Mater.* **2010**, *22*, 592.
[24] R. D. Farahani, H. Dalir, V. L. Borgne, L. A. Gautier, M. A. E. Khakani, M. Lévesque, D. Therriault, *Nanotechnology* **2012**, *23*, 085502.
[25] D. Paul, J. Lawrence, J. Troell, *Polym. Eng. Sci.* **1970**, *10*, 70.
[26] G. Kraus, J. Gruver, *J. Appl. Polym. Sci.* **1967**, *11*, 2121.
[27] M. M. Denn, *Annu. Rev. Fluid Mech.* **2001**, *33*, 265.
[28] E. Miller, J. P. Rothstein, *Rheol. Acta* **2004**, *44*, 160.
[29] G. A. Kouzaev, *Applications of Advanced Electromanetics: Components and Systems.*, Springer,Berlin–Heidelberg, Germany **2013**, pp. 1–49.